Effects of radiation on spectra, gradients, and preheat in laser-produced plasmas

D. Duston, R. W. Clark, and J. Davis
Plasma Physics Division, Plasma Radiation Branch, Naval Research Laboratory, Washington, D.C. 20375
(Received 8 January 1985)

Energy transport and photon emission are theoretically investigated in laser-heated foil targets at medium laser irradiance, with use of a numerical model which treats hydrodynamics, ionization, and radiation in a completely self-consistent manner. The radiation model is a detailed, collisional radiative scheme which calculates explicitly the line, recombination, and bremsstrahlung emission in concert with a probabilistic photon transport method. The role of radiation transport in thin-foil targets was studied as a function of target thickness, target-Z, laser intensity, laser wavelength, and laser pulse width. Significant differences were found in the radiation preheat, x-ray conversion efficiency, and broadband frontside emission spectrum, as these parameters were varied. It is also demonstrated that photon emission, absorption, and transport play an important role in the accurate calculation of heat penetration, plasma temperature and density gradients, and ablation-surface—to—critical-surface separation distance, and that radiation can constitute a major energy-loss mechanism even in a low-Z target such as carbon.

I. INTRODUCTION

The interaction of an intense short-wavelength laser beam with a solid foil target is a topic which has been studied vigorously for many years now (see, for example, Refs. 1—18 and their included references); however, many inherent problems still exist in our understanding of observed experimental data. In particular, the problem of transport through the target material of the deposited laser energy continues to attract much attention in the plasma physics community. Most of the work to date in this area has concentrated on particle transport, either by thermal or suprathermal electrons, and several theories have been proposed which deal with both limiting or enhancing the heat flux via particle flow. However, it is only very recently that workers have begun reporting on the effects of radiation transport in laser-heated targets in more than a merely qualitative way.[9,13,14,17—21] In spite of this recent attention, most studies have treated the atomic physics, ionization dynamics, and radiative transfer via approximate modeling techniques, invoking simplifying assumptions such as Saha or corona equilibrium, Rosseland mean opacities, and multigroup photon diffusion approximations. In a previous paper[22] (hereafter referred to as I) we described a new radiation-hydrodynamics model which included, for the first time, a collisional-radiative equilibrium (CRE) treatment of the ionization balance, a detailed configuration accounting (DCA) of the atomic level structure, and a novel radiation transport model based on a combination of probabilistic and frequency-by-frequency ray-trace techniques. In addition to documenting this model in I, we also addressed the problem of the heating of a thin aluminum foil by a relatively-low-irradiance (10^{13} W/cm^2) laser beam. In that study, we emphasized the role of the photon transport in the foil as an energy transfer mechanism, as well as discussing the emitted radiation spectrum in terms of both its energetic and diagnostic aspects.

In this paper, we continue our investigation of the role of atomic physics and radiative emission in laser-produced plasmas by studying the effects of these physical processes as a function of varying initial conditions. Using the same computer model as was employed in I, the laser characteristics and foil target properties are varied to determine their impact on the shape of the emitted spectrum, the temperature and density profiles, the radiative conversion efficiency, and the energy transport through the foil (as it affects the backside heating beyond the ablation surface and the rearside radiation spectrum). As in I, we conduct the investigation at irradiances lower than those required for significant suprathermal electron generation and thermal electron flux limiting. However, this should not impair our ability to make relative comparisons of the radiation transport effects in the various calculations and to draw meaningful conclusions from them regarding the radiative nature of laser-heated foils.

II. PROPOSED INVESTIGATION

In I, a single experiment was considered in detail and the nature of energy transport in laser-produced plasmas for one set of initial conditions explored. In this study we vary these initial conditions and examine the response of the plasma, as reflected in the characteristic radiation emission, to different parameters. One set of conditions is designated as the "standard" by which we will measure the variations in the other calculations. The initial conditions for the standard calculation were set at 0.35 μm laser wavelength, 10^{13} W/cm^2 peak laser irradiance, $\sim$3.0 nsec (FWHM) Gaussian laser pulse, incident on an 8-μm thick aluminum foil. The only difference between this standard calculation and that in I is the λ_l, the laser wavelength, which was 1.05 μm in that study. We chose to use frequency-tripled Nd:glass laser light for this investiga-

TABLE I. Initial conditions assumed for the six laser-heated foil calculations discussed in this investigation. Also, the total, broadband radiation conversion efficiency is given in the last column for each case.

Run	Laser irradiance W/cm^2	Laser pulse width (nsec)	Laser wavelength (μm)	Target material	Target thickness (μm)	Radiation conversion efficiency (%)
1	10^{13}	3.0	0.35	Al	8.0	30.7
2	10^{13}	3.0	0.35	C	8.0	18.8
3	10^{14}	3.0	0.35	Al	8.0	37.8
4	10^{13}	3.0	1.05	Al	8.0	26.7
5	10^{13}	3.0	0.35	Al	4.0	29.7
6	2×10^{13}	1.5	0.35	Al	8.0	27.1

tion because of its increased relevance to most recent studies in laser-plasma interaction. The advantages of higher frequency laser drivers have been discussed in several recent papers.[5–7,11–13,19]

In addition to the standard calculation, five other simulations were performed to study the variation of each of the initial conditions. The second calculation was intended to study the effect of changing the target material. Since the atomic model for carbon has also been completed with significant level structure and detail to be comparable with our aluminum model, that material was selected. The study of the response of a carbon target was of particular interest to us since radiation emission and transport is often neglected by workers studying laser-produced carbon targets under the assumption that lower-Z materials (like carbon) are quickly stripped of their bound electrons and, therefore, radiation contributes negligibly to the plasma dynamics and energy transport in these light targets. We sought, therefore, to either disprove or validate this common assumption conclusively with this calculation. In the third calculation, the laser irradiance was increased from 10^{13} to 10^{14} W/cm^2 while holding the pulse width fixed; thus, the deposition energy was increased by a factor of 10. Although treatment of suprathermal electrons and the invoking of a thermal flux limit becomes necessary at high irradiance, both of these mechanisms should have a negligible effect on the plasma dynamics at $\lambda_l=0.35$ μm and $I_l=10^{14}$ W/cm^2 and the results for this calculation should be valid. The fourth calculation was identical to the first but with the laser wavelength set to 1.05 μm, to allow us to determine the effect of driver frequency on the spectrum. The fifth calculation was performed to study the effects of thinner targets, hence, the aluminum foil thickness was reduced to 4 μm. In the sixth calculation, we examined the effect of more rapid deposition of laser energy by reducing the pulse width by $\frac{1}{2}$ to 1.5 nsec; to maintain the total deposited energy at a fixed value consistent with the standard calculation, the irradiance was doubled to 2×10^{13} W/cm^2.

A summary of the initial conditions for each of the calculations is given in Table I; the key from this table will often be used throughout the paper to designate a particular calculation.

III. THEORETICAL MODEL

The radiation-hydrodynamics model used for this study was thoroughly documented in I (and other related papers referenced therein) and we present only a brief description of it here; those wishing more information than presented here on the details of the physics included and the equations solved in the model are referred to the previous work.

The equations of hydrodynamics (transport of mass, momentum, and total energy) are solved in one-dimensional, planar geometry using a sliding-zone version of flux-corrected transport. We employ a special Lagrangian gridding which allows for sliding of the mesh so as to resolve steep gradients in the ablation region. This allows us to minimize the total number of zones while maintaining fine resolution in the region of steep temperature and density gradients. The model employs a single particle temperature, ideal equation of state (densities were never more than a few times solid), and classical thermal conductivity, solved in an implicit scheme. Laser absorption is via classical inverse bremsstrahlung, and any laser energy not absorbed by the time it reaches the zone containing the critical surface is dumped there.

The ionization model is based on collisional-radiative equilibrium (CRE) (Ref. 23) in which the population densities of ground and excited states are calculated by considering the most important particle and photon collisional processes populating them and solving for a time-independent solution of the set of atomic rate equations. A detailed atomic level structure for aluminum[24] is used which includes all 14 ground states, 84 excited levels, 97 free-bound continuum edges, and 144 averaged emission lines (more than 3000 nl transitions have been included).

The carbon model has not been as thoroughly documented as the aluminum one but includes all 7 ground states, 50 excited states, 56 free-bound continuum edges, and 107 averaged emission lines. The level structure for carbon is as complete as for aluminum but, of course, has fewer ions and consequently fewer excited states and lines. The collisional processes treated in the model include electron impact excitation and deexcitation, electron impact ionization and recombination, radiative recombination, dielectronic recombination, and spontaneous radiative de-

cay. The radiation transport algorithm is based on a combination of probabilistic[25] and frequency-by-frequency ray-trace[26] techniques and takes account of photoionization, inverse bremsstrahlung (of nonlaser photons), photoexcitation and stimulated emission processes. Of extreme importance in stopping the soft x rays in the dense foil regions is inner-shell opacity due to photoionization of inner-orbit electrons. This is treated along with the valence-electron photoionization scheme in a unique way[22] that allows the absorption edges to shift as the dense region heats up and ionizes. The opacity calculation is solved iteratively at each time step with the ionization calculation. Thus, the radiative transfer scheme treats opacity in the plasma self-consistently with the ionization dynamics and hydrodynamics.

As a check on the zoning algorithm, and to ensure adequate resolution in the regions of steep temperature and density gradients, a test calculation was performed with identical conditions as Run 1 but with the number of computational zones doubled. The comparison between the results of the two calculations was excellent: less than 5% difference in the total radiation output and a maximum of 25% error in the temperature and density profiles, but typically about 5%. This latter factor was the figure of merit everywhere except the region just outside the critical surface, indicating slight differences in local laser energy absorption with a finer mesh zoning. This should have little impact on the radiation energetics, however.

The model in its present form emphasizes and focuses the radiative properties and effects of laser produced plasmas. We have commented already on a number of approximations inherent in the model and are aware of some of the shortcomings and limitations imposed by them. However, we believe that within the regions of validity of the model that the results are reliable and the relative comparison of code results are quantitative as well as qualitative.

IV. DISCUSSION

In this section, the differences in the radiation characteristics of the laser-heated foils as a function of initial conditions are discussed. As in I, the various aspects of the emission we will be concerned with are the effects on (1) the radiation power as a function of time, (2) the temporal behavior of the backside temperature, (3) the forward and rearward directed radiation spectrum, and (4) the spatial temperature and density profiles inside the foil plasma. However, the most interesting results of this study were those obtained for the carbon foil; hence, we begin our discussion with the data from this calculation.

A. Laser-heated carbon foil

In I, it was pointed out that the energy distribution in the plasma was such that over 25% of the laser input energy was lost as radiative emission, almost all of this in the forward direction, toward the incident laser beam. From this it was clear that the neglect of radiation in the model would be a clear omission of a significant loss mechanism, and that radiation most probably affects the spatial distributions of temperature and density. This last point is verified in this investigation and will be discussed in detail later in this section. However, while acknowledging the effects of radiation on medium- and high-Z plasmas, it has long been the contention of many workers that radiation is a negligible loss mechanism in low-Z plasmas, such as carbon and boron. One supposes that this belief is based on the assumption that the laser energy quickly strips the low-Z target of its bound electrons, whence, the line emission power drops off rapidly and the total radiation becomes negligible in the description of the plasma dynamics. As a consequence of this assumption, many simulations have been performed in the past using carbon or plastic targets (plastic is a common ablator material in microballoon compression experiments) in which little or no account has been taken of the radiative processes, and quantitative results and conclusions have been drawn from these calculations regarding hydrodynamic instabilities, thermal smoothing, critical and ablation surface separation, ablation velocities, thermal front penetration, etc. Although this assumption may be justified in extremely thin foils, this study of a carbon foil target was designed to clarify this assumption for foils thicker than a few microns.

The initial conditions are those as shown in Table I for Run 2 (identical to the standard Run 1 with a carbon target substituted for an aluminum one). The laser pulse (which peaks at 4 nsec after initiation of the calculation) and the temporal behavior of the total radiation pulse is shown in Fig. 1 for the aluminum target (1) and the carbon target (2). Note the difference in the profiles. Although carbon exhibits a lower peak intensity and it occurs at an earlier time than in the aluminum curves, the close correspondence with aluminum on the rising part of the curve suggests that a simple "clipping" effect has taken place for $t \geq t_{\text{peak}}$ for the carbon curve. The explanation is straightforward: at 4.5 nsec, the electron temperature in much of the carbon plasma is above 100 eV, and

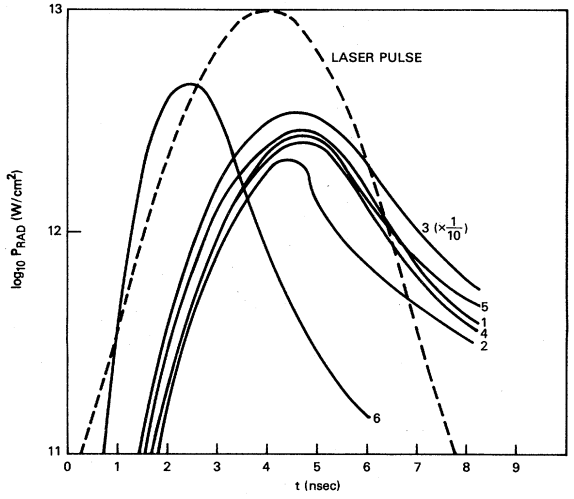

FIG. 1. The total radiated power is shown as a function of time for the six cases given in Table I. For reference, the laser pulse for Runs 1–5 is also shown (dashed curve).

the total radiation power output has begun to decrease (see Fig. 6). Put quite simply, most of the ablating plasma has been ionized down to C VI and C VII and the line and recombination radiation has degraded at this laser intensity. A target with more bound electrons might display a radiative response quite similar to the aluminum curve. Nevertheless, the total radiation conversion efficiency for these conditions is almost 20% for carbon (Table I).

To examine the radiative characteristics of each target more closely, we plotted the foil frontside spectra in Figs. 2 (aluminum) and 3 (carbon). Note that the photon energy axes of each figure differ by a factor of 10. As expected, the bulk of the emission for carbon is at much lower frequencies than that of aluminum. Although the line emission for aluminum is more intense than for carbon, the bound-free continuum is less intense. Quantitatively, a breakdown of the total radiated energy for aluminum gives about 32% in lines, 61% in bound-free continuum, and 7% in bremsstrahlung. The same breakdown for carbon gives only 11% in lines, 84% in bound-free continuum, and 5% in bremsstrahlung. Hence, the radiative recombination processes compensate for the decrease in line emission from carbon. This is easily understood from consideration of ionization dynamics. The line emission usually begins to depart from a strict N^2 (where N is density) dependence at lower densities than the bound-free radiation. This departure marks the onset of electron collisional quenching for each process. This is why the continuum dominates in laser plasmas (for low- and medium-Z materials) but line emission dominates in tokamak, gas-puff, and wire implosion plasmas. However, the density at which the quenching commences increases with increasing Z. Thus, in a laser-produced carbon plasma, the lines are more collisionally quenched than in an aluminum plasma but the continuum still scales approximately as N^2 and is below the quenching density. The reason why the carbon continuum intensity slightly exceeds (by 30%) the aluminum continuum is partly atomic structural differences. The carbon continuum is mostly due to recombination into K-shell levels while the aluminum continuum comes from L-shell recombinations. Since the lower charge state radiation becomes collisionally quenched at lower densities than those of the K-shell, the carbon continuum exceeds that of the aluminum. Also, the ion density near the critical surface, where most of the radiation is emitted, is higher for carbon (which has fewer free electrons) than for the aluminum plasma, which brings into play once again the N^2 scaling of the continuum radiation.

Now that it has been shown that the total radiative emission from carbon is a significant energy loss mechanism, we want to determine whether the radiation causes modifications in the spatial temperature and density profile, as well. Thus, the carbon calculation was compared with an identical run in which the radiation loss term was omitted, i.e., a "hydro-only" calculation was performed.

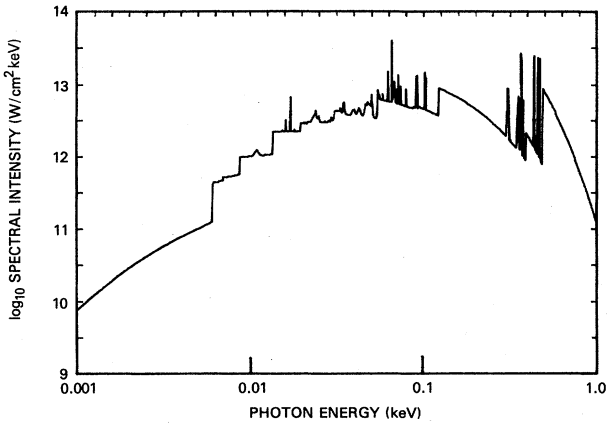

FIG. 3. The frontside radiation power spectrum for Run 2 (the carbon foil calculation) at 4.5 nsec, near the peak in the radiation pulse. Note that the x axis differs from that in Fig. 2.

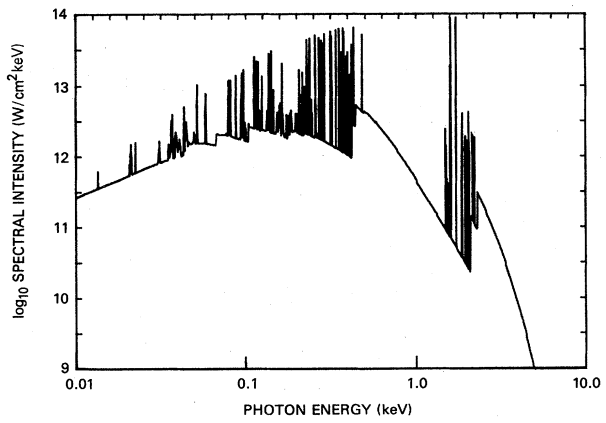

FIG. 2. The frontside radiation power spectrum for Run 1 (the "standard" aluminum run), at 4.5 nsec, near the peak in the radiation pulse.

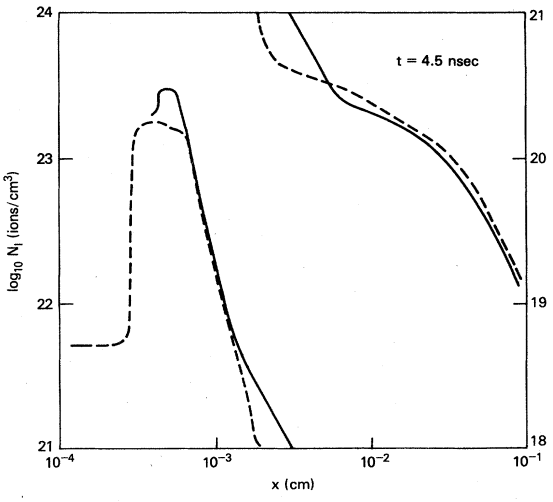

FIG. 4. Ion density profile for the laser-heated carbon foil study (Run 2) at 4.5 nsec. The solid line is the complete radiation/hydrodynamic calculation, while the dashed curve is neglecting radiation loss ("hydro only").

To ensure that the two runs were otherwise identical, the same ionization dynamics were employed for both. The ion-density profile as a function of distance, x, is shown for both calculations in Fig. 4; the time of this plasma "snapshot" was 4.5 nsec, corresponding to the peak in the radiation pulse. The values of x in each curve (and in successive similar figures) were adjusted in order that the ablation surfaces would coincide. This was necessary since the predicted foil acceleration is slightly greater when radiation is neglected. In fact, the predicted velocity of the rearside of the foil is about 50% greater when no radiation is included. This accounts for the 4-μm difference in the position of the backside of the foil plasma, as well as for the slightly higher peak density in that calculation which included radiation. Note that the density gradient is steeper in the "hydro-only" calculation, and, as a consequence, the density in the ablation region is *lower* by a factor of 2.5. Both calculations are in good agreement, however, far out in the blowoff region beyond the critical surface, located at a density of about 1.6×10^{20} ions/cm^3.

In Fig. 5, the temperature profiles are shown for the same two calculations; note that the largest disagreement also occurs in the ablation region and extends past the critical surface. In fact, including an accurate accounting of the radiative loss increases the prediced ablation surface-to-critical surface separation from 11 to 18 μm. The quantitative difference in internal energy between the two runs at this time (4.5 nsec) is 48% of the energy deposited for "hydro-only" versus 38% with the radiation included. The kinetic energy is also higher (41% versus 32%), while the potential energy stored in ionization and excitation is virtually identical in both runs. Thus, with no account of the radiative losses in the foil plasma, one would, in general, predict hotter temperatures and greater acceleration. This fact becomes most apparent when attempting to model thermal conduction in the ablation region. Simulations that do not include an accurate description of local radiation loss will calculate temperatures which are much higher than they are in reality, which could lead to invalid conclusions about the mode of energy transport through the ablation surface. As seen in Fig. 5, there is a discrepancy of as much as 150 eV near the critical surface, due entirely to neglecting radiation. Thus if one wishes to model an experiment accurately, it seems pointless to embark upon a calculation using a sophisticated thermal conduction scheme if equal attention is not paid to the details of the radiation modeling.

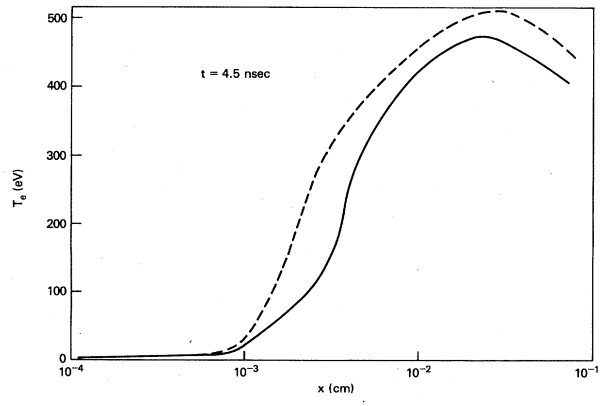

FIG. 5. Temperature profile for the laser-heated carbon foil study (Run 2) at 4.5 nsec. The solid line is the complete radiation/hydrodynamic calculation, while the dashed curve is neglecting radiation loss ("hydro only").

B. Aluminum radiation power

As discussed in the previous section, the total radiation energy in laser-produced carbon foils is a rather substantial fraction of the total deposited energy and can significantly affect the spatial profiles of plasma parameters in certain regions. As would be expected, this is even more true as the Z of the target is increased. From Table I and Fig. 1, we see that the aluminum foil (Run 1) is a slightly better radiator than the carbon foil (Run 2). In addition, a "hydro-only" run for the same initial conditions as Run 1 yielded much the same result as was found with carbon: much gentler gradients in the ablation region when accurate radiation modeling is included, in addition to significantly lower temperatures in the region near the critical surface. Thus, the statements made earlier about modeling carbon plasmas are even more valid for aluminum.

Comparing the other conversion efficiencies in Table I, we find only a weak dependence on the laser wavelength (up to 1 μm light, at least), foil thickness, and laser pulse width. Of course, if the initial parameters were changed significantly from the range in Table I, this might not be the case. If, for example, the foil thickness was reduced to 2 μm or less, the reduced mass may allow for such high temperatures that the material becomes fully ionized with the result that the radiative emission drops precipitously. From the higher irradiance calculation (Run 3), a significant increase in radiative efficiency was found. Although a scaling law is not very reliable when based on two points, the radiative output appears to vary as approximately $I_l^{1.1}$. It would have been interesting to extend the irradiance range to 10^{15} W/cm^2, but the validity of the model would be questionable at this value for reasons discussed in Sec. III. From Fig. 1 we see that the time history of the radiation pulse is nearly identical for all initial conditions, with the exception, of course, of the shortened laser pulse calculation (Run 6). Here the radiation is emitted with only a 64% increase in the peak intensity (the irradiance was 100% greater) but the radiation pulse width (FWHM) only decreased by 40%, giving a total yield of only slightly less than the longer pulse-width calculation. The laser-heated carbon foil shows a slight deviation from the other curves after peak intensity is reached at 4.5 nsec; this is due to combined plasma and atomic physics phenomena. Most of the radiation that escapes the plasma emanates from the region near the critical surface, and slightly outside of it. The temperature in this region is higher for the aluminum target ($\sim$170 eV) than for the carbon target ($\sim$115 eV), since the ion density at critical is typically greater for carbon than for aluminum. After 4.5 nsec, the electron temperature begins decreasing in this region. As shown in Fig. 6, where the radiative power coefficient (radiated power per ion per electron) is

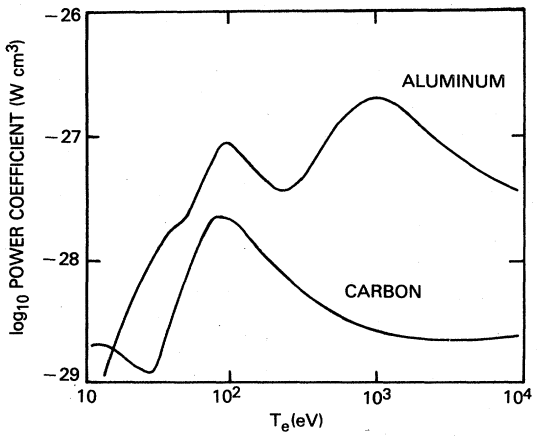

FIG. 6. Total radiative cooling power coefficient for aluminum and carbon plasmas versus electron temperature, at a density of 10^{20} ions/cm^3.

plotted versus electron temperature, both materials have a relative maximum in their equilibrium radiation yields near 100 eV temperature, corresponding to a maximum in the *K*-shell yield for carbon and the *L*-shell yield for aluminum. Thus, as the aluminum target falls from 170 eV toward 100 eV, its radiative power coefficient is *increasing*. On the other hand, as the carbon target falls from 115 eV through 100 eV, its radiative power coefficient begins *decreasing*. Thus, a more rapid drop in carbon radiation is evident at 5 nsec. This trend is reversed at 6.5 nsec, since the dropping temperatures now put the carbon plasma onto the *L*-shell radiation peak (the power coefficient begins increasing again at about 40 eV), whereas the aluminum coefficient is still decreasing on the low-temperature side of the *L*-shell peak. Of course, both power curves are monotonically decreasing as the foil blows apart and ion density decreases, but, as seen in Fig. 1, the atomic structure of the target can cause slight differences in the temporal variation of the emitted radiation.

C. Aluminum forward radiation spectra

Earlier, the forward-directed radiation spectra for the standard aluminum calculation was compared with that for a carbon target under identical initial conditions (see Figs. 2 and 3) and predictably, significant differences were found due mainly to the vast differences in atomic structure. On the other hand, it was not as easy to predict what differences, if any, would appear in the spectra of the other four calculations (Runs 3—6) as compared to Run 1. Considering, first, the spectrum from the 10^{14} W/cm^2 calculation, it is expected, in light of the increase in radiative output, that the spectrum would be more intense overall. As seen in Fig. 7, this is the case; to assist in comparison, the continuum base line from Fig. 2 (the "standard" spectrum) is shown as a dashed line. A number of interesting features are seen: (1) greater differences are prevalent at higher photon energies than at lower, indicating a hotter plasma, (2) the hydrogenlike lines are much more intense than the heliumlike lines, at about 1.6—1.8 keV, indicating a hotter blowoff plasma,

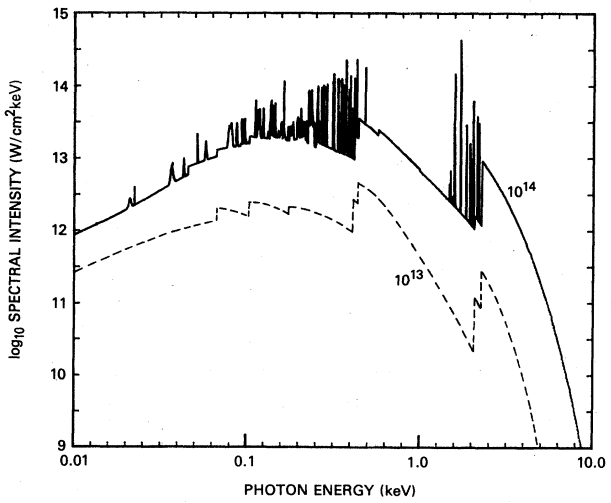

FIG. 7. The frontside radiation power spectrum for the laser-heated aluminum foil study at 10^{14} W/cm^2 laser intensity (Run 3) at 4.5 nsec. The continuum base line for the 10^{13} W/cm^2 calculation (Run 1) is shown for reference (dashed curve).

and (3) relatively more intense line emission is evident in Fig. 2 than in Fig. 7, indicating higher densities in the line-emitting region for the high irradiance run. To verify this last point, the actual breakdown by atomic process was checked. As stated earlier for the standard run, the line emission was 32% of the total, while radiative recombination was 61% and bremsstrahlung 7%. For the high irradiance study, line emission was only 18%, recombination was 73%, and bremsstrahlung 9%. Since the recombination radiation tends to intensify with respect to line emission in dense plasma, the conclusion is that the strongly emitting region is denser in the high irradiance calculation. We see that this is the case in Fig. 8, where

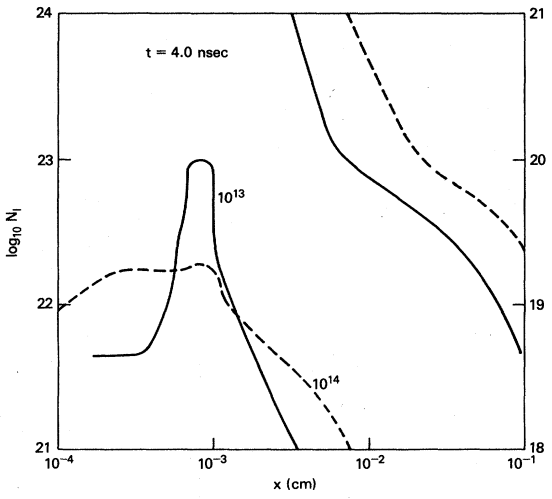

FIG. 8. Ion density profile for the laser-heated aluminum foil studies at 10^{13} W/cm^2 (Run 1) and 10^{14} W/cm^2 (Run 3) laser irradiance, at 4.0 nsec.

the ion density profiles for both Run 1 and Run 3 are shown for $t=4.0$ nsec. Most of the emission comes from the range 40 to 80 μm, and the density is clearly higher in that region for the high irradiance case; as is well known, the mass ablation rate is greater at higher irradiance and, hence, so is the density in the ablation and underdense region. Of course, the mass must come from somewhere, and that place is the dense region behind the ablation surface as shown in the figure. Temperatures are everywhere higher for the high irradiance calculation at this time except near the critical surface region, as shown in Fig. 9. This explains why the lower-energy photons in Fig. 7 do not scale as strongly as those at higher energy: there is no longer a low-temperature region $T<10$ eV in the foil. Since there is a limit to how much mass of a finite thickness foil can be ablated before burning through the foil, and because the aluminum atoms may eventually be completely ionized with the higher temperatures attained by added energy deposition, it is questionable how much higher the irradiance could be increased and still expect an almost linear increase in radiation. Although it would be possible to determine this using the model, the results may not be valid due to the onset of other physical processes at these higher laser powers.

Turning now to the other three aluminum studies, it was found that the frontside spectra were very similar to the standard calculation in the basic shape of the continuum and only slight differences in line emission were apparent. For the calculation in which the laser deposition time was decreased (Run 6), the broadband intensity was greater due to the higher laser intensity, but the only real qualitative difference in the spectral distribution was in the K lines, which displayed enhanced hydrogenlike emission compared to heliumlike emission. This is consistent with the hotter temperatures which existed in the blowoff due to the higher laser irradiance. Similarly, the calculation in which the laser wavelength was raised to 1.06 μm (Run 4) predicted an identical spectrum with the exception of the same effect in the K lines as noted above. In this case, the hotter temperatures in the blowoff are due to the lower critical density corresponding to 1 μm light; since the energy is deposited at lower densities, the plasma corona is warmer resulting in an enhancement of the Al XIII emission. In the case of the 4-μm-thick aluminum foil, no discernible differences in the frontside spectra were noted except small variations in a few of the L lines and a slightly higher continuum level at low frequency for the thinner foil case. This is due to the higher temperatures in the highly dense region of the thinner foil, a product of greater radiation preheat. This trend of higher backside temperatures should continue as the foil thickness is decreased (a result verified experimentally by McLean *et al.*[3]). A more detailed discussion of this follows in the next section.

D. Aluminum rearward radiation spectra

An analysis of the rearward directed radiation emission can be very illuminating in the sense that it not only shows the extent of radiation preheat that can be expected, but one can deduce the amount of radiation deposited in the foil (and, hence, the role of radiation transport internal to the plasma) by noting the difference between frontside and backside spectra. In Fig. 10, the backside spectra are shown for the standard aluminum calculation (at 10^{13} W/cm^2) and the higher irradiance (10^{14} W/cm^2) aluminum calculation (Run 3). The standard run (shown as a dashed curve) has only a high-energy component corresponding to "shine-through" radiation, photons from the hot frontside plasma that have not been attenuated by the dense backside. The sharp cutoff at about 1.56 keV is due to the K absorption edge; the very intense peaks are due to $K\alpha$ emission from the dense backside and are probably less intense than shown due to the omission of resonant $K\alpha$ self-absorption effects in the model. The

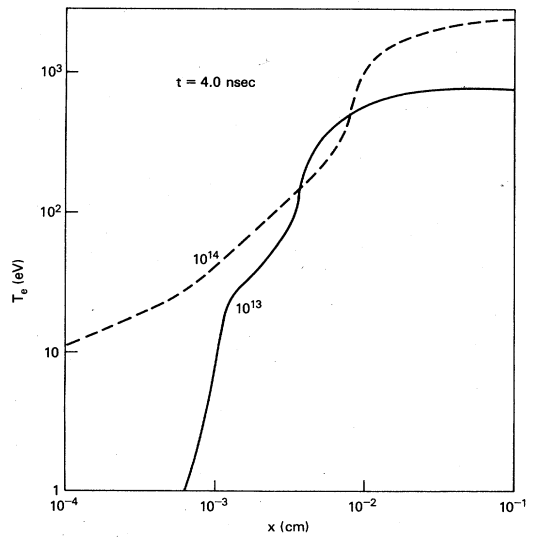

FIG. 9. Temperature profile for the laser-heated aluminum foil studies at 10^{13} W/cm^2 (Run 1) and 10^{14} W/cm^2 (Run 3) laser irradiance, at 4.0 nsec.

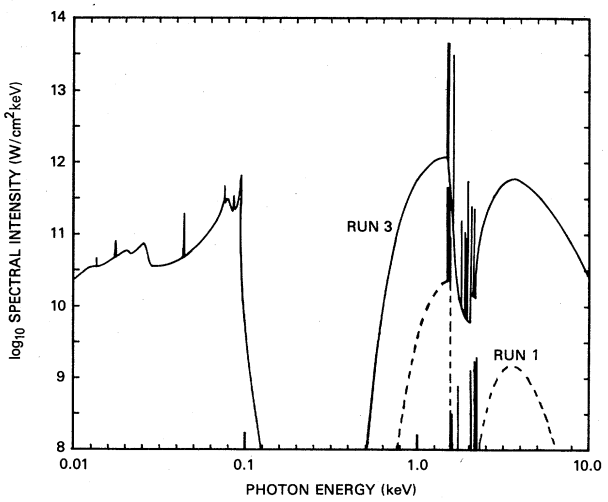

FIG. 10. Backside radiation power spectrum for the laser-heated aluminum foil studies at 10^{13} W/cm^2 and 10^{14} W/cm^2 laser irradiance, at 4.5 nsec.

low-energy feature below 0.1 keV is due to two different components. The first is shine-through radiation from in front of the ablation surface, mostly radiative recombination. This emission is superimposed on another component, mostly bremsstrahlung, which originates directly from the foil backside. Although it is dominated by the recombination photons, this true backside radiation closely resembles a blackbody emission curve for a plasma at a temperature approximately equal to the rearside electron temperature. At lower laser irradiances it was found that the bremsstrahlung component dominated, and, by assuming a blackbody emission profile, diagnostic measurements of the rearside spectra at low photon frequencies could be used to determine the backside temperature. However, at higher irradiances, we see that the technique is rendered invalid by the highly non-Planckian bound-free shine-through radiation. Note that while the intensity level of both the low- and high-energy components is about equal for the high-irradiance case, the low-energy component is well below (off scale) the high-energy photon intensity for the standard aluminum run. This is due to the difference in backside temperatures of the two foils, about 10 eV for the 10^{14} W/cm^2 case and only 1.5 eV for the 10^{13} W/cm^2 case. Once again, the effects of radiation transport have a profound effect on the preheat and radiative shine-through.

The backside spectra from two of the other three aluminum calculations were rather similar to the standard run. The calculation using 1-μm laser light (Run 4) was, in fact, virtually indistinguishable from the 0.35-μm study, demonstrating that for sufficiently thick foils, the radiation preheat and shine-through is somewhat insensitive to the laser frequency. The rearside spectrum for the 4-μm-thick aluminum foil (Run 5), shown in Fig. 11 (upper trace), has both an intense low-frequency feature as well as a broader, more intense high-energy component when compared to the standard 8-μm foil. Both effects are due to a significant reduction in opacity as foil thickness is decreased; this leads to increased shine-through as well as an increase in actual rearside bremsstrahlung, owing to the higher electron temperatures (about 3.5 eV) there. The rear spectrum for the 1.5-nsec pulse-width calculations (Run 6), also shown in Fig. 11 (lower trace) at a time of 2.0 nsec exhibits a high-energy photon component identical in shape, but just a bit more intense than the standard 3-nsec calculation. This is due to the greater irradiance (2×10^{13} W/cm^3) used for this calculation; the rearside temperature is slightly higher than in the standard run which reduces the opacity slightly allowing for more transmission of the superkilovolt radiation. However, the low-energy component is missing for these conditions, also.

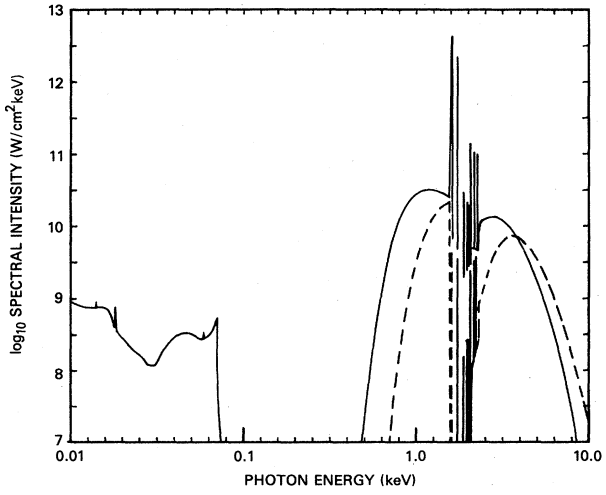

FIG. 11. Backside radiation power spectrum for two laser-heated aluminum foil studies, Run 5 the 4-μm-thick target (solid curve) and Run 6 the 1.5-nsec laser pulse width (dashed curve).

In conclusion, it is worth discussing a few points concerning the low-energy component of the backside spectra. Only two of the five aluminum calculations performed displayed this feature with intensities (but not energy) comparable to the higher-energy emission: (1) the high irradiance run and (2) the thin, 4-μm-foil run. In both cases, this feature was comprised of both a bremsstrahlung component which was true backside emission and a low-energy radiative recombination component, some shining through from in front of the ablation surface, and some coming directly from the backside. It appears that these components may be irrevocably linked; namely, if the backside has been heated to temperatures high enough to emit strongly, then, by definition, the plasma opacity has dropped sufficiently that the shine-through component is also fairly intense.

E. Aluminum plasma profiles

In Sec. IV A, comparisons were made between carbon foil calculations for which the radiation emission was both included and neglected as an energy transport mechanism, and significant differences in the two runs were discussed. We would like to now show a similar comparison made for the standard set of initial conditions in an aluminum target, and discuss in greater depth the radiation transport mechanism in the plasma. For this study, two additional calculations were carried out for the conditions of Run 1. Run 1A was identical to Run 1 but the plasma was treated as optically thin; that is, the cooling rate was overestimated by allowing *all* emitted radiation to escape the plasma. Run 1B was also identical to Run 1, but was a "hydro only" calculation, in which no radiation cooling was taken into account. The plasma density and temperature profiles at a time of 4.0 nsec (laser peak) are shown for all three cases in Figs. 12 and 13. The profiles have been adjusted in position, χ, so that the ablation surfaces coincide in space. In the dense region behind the ablation surface, the three calculations show very little difference in the predicted ion densities except in the degree of rearside ablation, which varies over about 6 μm from run to run at this time. In the far underdense plasma ($\chi > 8\times10^{-3}$cm) where the density is less than 10^{20} ions/cm^3, the differences in the calculations are essentially small. However, in the ablation and critical regions ($10 < \chi < 80$ μm) the results vary significantly; most notably, the density gradient for the complete

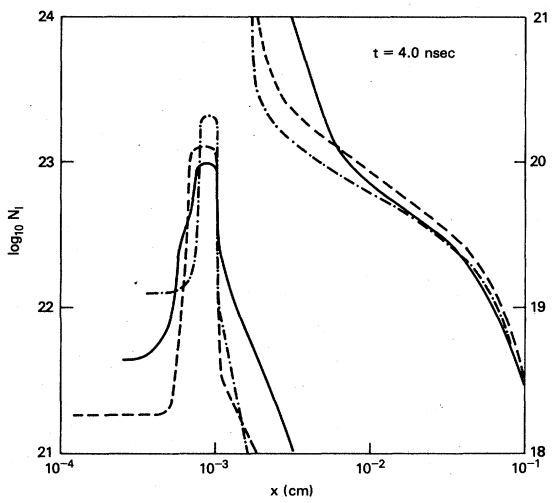

FIG. 12. Ion density profile for the laser-heated aluminum foil studies at 4.0 nsec; the conditions are those of Run 1. Shown are the results for the complete calculation (solid curve), the optically thin calculation (dashed-dotted curve), and the "hydro only" (no radiational cooling) calculation (dashed curve).

radiation/hydrodynamics calculation has a much longer scale length than either the "hydro-only" or "optically thin" models predict. As a consequence of this, the predicted ablation surface-to-critical surface separation distance increases from about 6.0 to 10.0 μm in the optically thin and pure hydro runs to 23 μm in the complete run. Obviously, radiation transport plays an important role in reducing the gradient and, thus, can significantly affect the calculation of mass ablation rates, thermal conduction, and electron penetration as well as instability growth in the ablation region. For this reason, accurate radiation transport algorithms and, consequently, detailed atomic models are a requirement of accurate modeling.

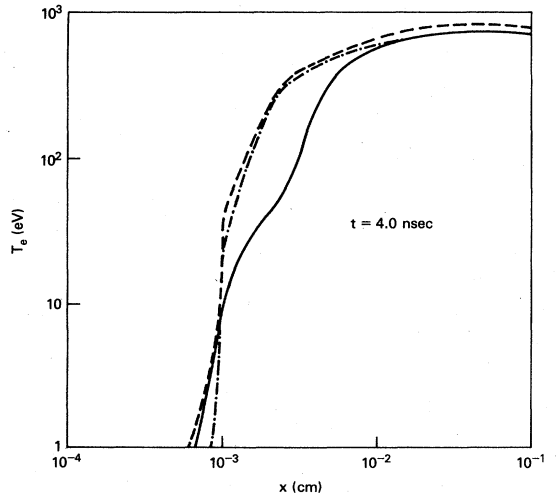

FIG. 13. Temperature profile for the laser-heated aluminum foil studies at 4.0 nsec. The three curves correspond to those described in Fig. 12.

The mechanism by which the radiation modifies the density profile is straightforward. (1) The largest net photon emission rates are found very near the critical surface, where they serve to cool this region. (2) The radiation energy is transported back toward the laser (where most escapes through the essentially optically thin blowoff) and also inward toward the ablation surface where it is strongly absorbed, causing heating. (3) The increased temperature (and, hence, pressure) in the ablation region translates into greater mass ablation toward critical. (4) This ablation is aided by the reduced temperature in the radiatively cooled critical region, since there is less back-pressure to inhibit the flow. Thus, the temperature and density gradients are much less steep due to the photon emission.

The importance of radiation energy transport into the dense backside plasma is illustrated via the optically thin calculation. Since radiation loss is included in the energy equation, the critical region is again strongly emitting. However, since trapping is not allowed, the backside is not preheated as much and the resulting mass ablation rate drops. This is shown in Fig. 12, by the fact that the density is very much lower for Run 1A than for Run 1. In fact, this preheat is so essential to the profile modification that even the pure hydro calculation, Run 1B, displays higher densities in this region than does the optically thin calculation. Based on recent theories and preliminary results of thermal conduction[17,19,27–35] in the ablation region and the prediction of a "thermal foot" which penetrates the ablation surface ahead of the main heat pulse, it is likely that these gradients will be further modified by more sophisticated treatment of the conduction processes. In fact, we speculate that the modification may be amplified by the *cooperative* effects of the radiation and electrons, since the thermal conduction preheat will facilitate the penetration of the x rays deeper into the dense region by reducing the optical depth (increasing the photon mean free path) there.

V. CONCLUSIONS

In the investigation reported on here, we have extended an earlier study of laser-heated foil targets by employing a well-documented numerical radiation/hydrodynamics model to study how varying laser and target conditions can affect the energy transport internal to and the radiation emitted from laser-driven plasmas. Since the main emphasis of this study was the plasma radiation energetics, we concentrated our modeling efforts on the ionization and transport schemes in order to obtain as accurate as possible a representation of the radiative emission. As a result of these studies, several important conclusions can be drawn.

First, it was irrefutably established that radiative transport and losses are a significant perturbation effect on the evolution of laser-heated foils, affecting not only the gross energy balance, but also decreasing temperature and density gradients in the critical region and increasing the predicted values for ablation-to-critical layer separation. That the radiation was a major loss mechanism in higher-Z plasmas was previously an accepted fact. However, it has been shown here to be equally important at

lower atomic number as well, providing that the low-Z target thickness is sufficiently large so as to prevent it from becoming totally ionized (although radiative recombination from the bare nucleus was also shown to be a powerful radiative process). At laser intensities of 10^{13} W/cm^2, e.g., the 8-μm carbon foil studied was in no danger of becoming fully stripped, and, hence, much thinner foils would have to be used in order to justify the neglect of the radiative loss in modeling calculations.

Since this study did not exceed laser irradiances of 10^{14} W/cm^2 for aluminum and 10^{13} W/cm^2 for carbon, an important question is the scaling of the x-ray emission at higher laser intensities. Previous studies on gold at 0.53 μm (Refs. 11 and 13) seem to give contradictory theoretical results but corroborating experimental numbers on the x-ray efficiency; both studies show (experimentally) a plateau for gold at about 10^{14} W/cm^2, while Mead *et al.*[13] predict a decrease in efficiency as the irradiance is increased from 3×10^{14} to 3×10^{15} W/cm^2. From Table I, we see a rise in conversion efficiency for aluminum targets from 30.7 to 37.8% as laser irradiance at 0.35 μm is increased from 10^{13} to 10^{14} but in our estimation this trend will reverse around 10^{15} W/cm^2. The laser intensity at which the efficiency saturates for carbon may be slightly lower; however, the radiation losses should still be considerable in the 10^{14}–10^{15}-W/cm^2 range for targets thick enough to avoid complete burn-through.

Although a decrease in x-ray conversion efficiency was found when the laser wavelength was increased to 1.05 μm in agreement with earlier experiments on gold,[11] the degradation (30.7% down to 26.7%) was not as large for our aluminum calculations as was measured for the gold targets. In addition, our conversion efficiencies were also slightly ($\sim$50%) higher than those calculated by Mead *et al.*[19] for aluminum. Possible reasons for the difference are (1) difference in laser pulse width (700 psec vs 3 nsec), (2) difference in photon energy range (subkilovolt vs total broadband), and (3) the use of a flux limit in their calculations. Of course, there are also significant differences in the ionization/radiation/transport models which could also account for this difference.

Almost no effect on the x-ray emission was found as the thickness of the foil was reduced from 8 to 4 μm. However, foil targets much thinner than this will be susceptible to increased ionization due to heat penetration and the resulting lower densities will cause a reduction in net photon flux escaping the plasma. Some decrease in conversion efficiency was evident as the laser pulse was shortened (30.7 to 27.1%) by a factor of 2. This would seem to explain some of the differences between this and other studies at shorter pulse widths, as described above.

Radiation from carbon targets was shown to produce a very different spectrum from that of aluminum under identical conditions. The photons were produced more by recombination and less by bound-bound transitions for carbon, and the radiation was emitted at generally lower energies. Recombination from the bare nucleus to ground and excited levels of hydrogenlike carbon was found to be a strong radiation process. Finally, the radiation preheat, as deduced from the backside spectrum was shown to be a strong function of laser irradiance and target thickness but only weakly dependent on the laser pulse width and wavelength, within the range of parameters studied here.

ACKNOWLEDGMENTS

We would like to thank Ted Cochran and John Apruzese for helpful suggestions regarding the numerical modeling of the hydrodynamics and the radiation transport, and Hans Griem for useful comments on the manuscript. This study was sponsored in part by the U.S. Defense Nuclear Agency and the U.S. Office of Naval Research.

[1]H. D. Shay *et al.*, Phys. Fluids **21**, 1634 (1978).
[2]B. H. Ripin *et al.*, Phys. Fluids **23**, 1012 (1980).
[3]E. A. McLean *et al.*, Phys. Rev. Lett. **45**, 1246 (1980).
[4]G. McClellan, P. H. Y. Lee, and G. Caporaso, Phys. Rev. Lett. **44**, 658 (1980).
[5]H. Nishimura *et al.*, Phys. Rev. A **23**, 2011 (1981).
[6]B. Yaakobi *et al.*, Opt. Commun. **38**, 196 (1981).
[7]B. Yaakobi *et al.*, Opt. Commun. **39**, 175 (1981).
[8]B. Yaakobi, J. Delettrez, L. M. Goldman, R. L. McCrory, W. Seka, and J. M. Soures, Opt. Commun. **41**, 355 (1982).
[9]N. G. Basov *et al.*, Kvant. Elektron. (Moscow) **9**, 1525 (1982) [Sov. J. Quant. Electron. **12**, 977 (1983)].
[10]P. Jaeglé, A. Carillon, and G. Jamelot, Phys. Rev. A **27**, 1247 (1983).
[11]H. Nishimura, F. Matsuoka, M. Yagi, K. Yamada, S. Nakai, G. H. McCall, and C. Yamanaka, Phys. Fluids **26**, 1688 (1983).
[12]M. H. Key, W. T. Toner, T. J. Goldsack, J. D. Kilkenny, S. A. Veats, P. F. Cunningham, and C. L. S. Lewis, Phys. Fluids **26**, 2011 (1983).
[13]W. C. Mead *et al.*, Phys. Fluids **26**, 2316 (1983).
[14]P. G. Burkhalter *et al.*, Phys. Fluids **26**, 3650 (1983).
[15]B. Meyer and G. Thiell, Phys. Fluids **27**, 302 (1984).
[16]M. J. Herbst *et al.*, Phys. Rev. Lett. **52**, 192 (1984).
[17]B. Yaakobi *et al.*, Phys. Fluids **27**, 516 (1984).
[18]J. L. Bocher, M. Decroisette, P. A. Holstein, M. Louis-Jacquet, B. Meyer, A. Saléres, and G. Thiell, Phys. Rev. Lett. **52**, 823 (1984).
[19]W. C. Mead *et al.*, Phys. Fluids **27**, 1301 (1984).
[20]E. N. Ragozin, Kvant. Elektron. (Moscow) **9**, 1346 (1982) [Sov. J. Quant. Electron. **12**, 856 (1982)].
[21]A. V. Vinogradov and B. N. Chichkov, Kvant. Elektron. (Moscow) **10**, 741 (1983) [Sov. J. Quant. Electron. **13**, 458 (1983)].
[22]D. Duston, R. W. Clark, J. Davis, and J. P. Apruzese, Phys. Rev. A **27**, 1441 (1983).
[23]D. R. Bates, A. E. Kingston, and R. W. P. McWhirter, Proc. R. Soc. London, Ser. A **267**, 297 (1962).
[24]D. Duston and J. Davis, Phys. Rev. A **23**, 2602 (1981).
[25]J. P. Apruzese, J. Davis, D. Duston, and K. G. Whitney, J.

Quant. Spectrosc. Radiat. Transfer **23**, 479 (1980).
[26]J. P. Apruzese, J. Davis, D. Duston, and R. W. Clark, Phys. Rev. A **29**, 246 (1984).
[27]A. R. Bell, R. G. Evans, and D. J. Nicholas, Phys. Rev. Lett. **46**, 243 (1981).
[28]D. Shvarts, J. Delettrez, R. L. McCrory, and C. P. Verdon, Phys. Rev. Lett. **47**, 247 (1981).
[29]R. J. Mason, Phys. Rev. Lett. **47**, 652 (1981).
[30]J. P. Matte and J. Virmont, Phys. Rev. Lett. **49**, 1936 (1982).
[31]A. R. Bell, Phys. Fluids **26**, 279 (1983).
[32]D. J. Bond, Phys. Lett. **88A**, 144 (1982).
[33]S. A. Khan and T. D. Rognlien, Phys. Fluids **24**, 1442 (1981).
[34]J. R. Albritton, Phys. Rev. Lett. **50**, 2078 (1983).
[35]J. F. Luciani, P. Mora, and J. Virmont, Phys. Rev. Lett. **51**, 1664 (1983).